Extended tissue tropism and vertical transmission in a murine model of Mayaro virus infection

Arévalo A.P.[1], Perbolianachis P.[2,3], Pórfido J.L.[1], Pereira-Gómez M.[2,4], Greif G.[5], Hurtado J.[2,3], Fajardo A.[2,3], Varela B.[6], Verdes J.M.[6], Moratorio G.[2,3*], Crispo M[1*].

[1]Laboratory Animal Biotechnology Unit, Institut Pasteur de Montevideo, Uruguay

[2]Experimental Virus Evolution Laboratory, Institut Pasteur de Montevideo, Uruguay

[3]Laboratory of Molecular Virology, Nuclear Research Center, Faculty of Sciences, Udelar

[4]Microbiology Unit, Department of Pathobiology, Faculty of Veterinary Medicine, Udelar

[5]Host-Pathogen Interaction Laboratory, Institut Pasteur de Montevideo, Uruguay

[6]Pathology Unit, Department of Pathobiology, Faculty of Veterinary, Udelar

[*] Corresponding authors: crispo@pasteur.edu.uy; moratorio@pasteur.edu.uy

Abstract

Mayaro (MAYV) virus, an emerging arthritogenic alphavirus of the *Togaviridae* family, represents a growing public health concern in Latin America due to its capacity for expansion into urban transmission cycles. In the absence of approved antivirals or vaccines, robust animal models are essential to investigate viral pathogenesis and evaluate

potential therapeutic strategies. While MAYV infection is primarily transmitted by mosquitoes, its tissue tropism, systemic dissemination, and potential non-vector transmission routes remain incompletely understood. Here, we establish a comprehensive murine model to investigate MAYV pathogenesis, with particular emphasis on reproductive tissues and gestational stages. Following intraperitoneal infection, MAYV rapidly disseminated to lymphoid, visceral, musculoskeletal, and reproductive organs, inducing hematological and biochemical alterations that mimics of human infection. In pregnant females, viral dissemination and host responses differed markedly according to gestational stage. Early pregnancy was characterized by placental permissiveness, fetal exposure, and transcriptional signatures associated with inflammation and antiviral responses, whereas mid gestation showed a more restricted placental profile. Infectious viral particles were also detected in reproductive tissues and enriched sperm samples, supporting the biological plausibility of sexual transmission. In addition, *in vivo* imaging using a luminescent MAYV reporter gene enabled real-time visualization of viral kinetics and tissue persistence. Together, these findings identify viral tropism, with gestational stages as a critical determinant of placental permissiveness and fetal exposure to MAYV, establishing a robust *in vivo* platform to study MAYV dissemination, transmission potential, and host–pathogen interactions.

Keywords: MAYV; Pathogenesis; Alphavirus; Emerging arbovirus; Vertical transmission; Pregnancy; Placenta; Murine model

Introduction

Mayaro virus, an emerging arbovirus of the *Alphavirus* genus and *Togaviridae* family, was first identified in Trinidad and Tobago in 1954 and has since been responsible for

45 sporadic outbreaks across Central and South America. Imported cases have also been
46 reported in Europe and North America, raising concerns at the international public health
47 level as reflected in the epidemiological alert issued by the Pan American Health
48 Organization / World Health Organization in May 2019, which emphasized the need to
49 strengthen epidemiological surveillance and laboratory diagnostic capacity (1). The virus
50 has already been detected in Brazil, Peru, Venezuela, Suriname, Colombia, Ecuador,
51 Bolivia, and Panama, with serological evidence also reported in Costa Rica, Guatemala,
52 Mexico, and Haiti (2–5). Multiple anthropogenic factors—including climate change,
53 urbanization, human mobility, and the expanding distribution of mosquito vectors such
54 as *Aedes aegypti* and *Aedes albopictus*—contribute to the increasing risk of MAYV
55 geographic expansion, even in countries without active transmission, such as Uruguay
56 (6,7). A recent study estimated that 58.9 million people in Latin America reside in
57 ecologically suitable areas for MAYV transmission (6,8). From a genomic perspective,
58 MAYV possesses a positive-sense single-stranded RNA genome of approximately 11.5
59 kb, which encodes both non-structural (nsP1–nsP4) and structural proteins (CP, E3, E2,
60 TF, 6k, and E1) through two open reading frames (ORFs). The virion is enveloped in a
61 lipid membrane containing E1 and E2 glycoproteins and exhibits high genetic plasticity,
62 which facilitates its adaptation to a broad range of hosts. The viral replication cycle begins
63 with the fusion of the viral envelope to the host cell membrane, followed by translation
64 of viral proteins and the assembly of new virions. MAYV is classified into three
65 genotypes: D (dispersed), L (limited), and N (new), the latter identified in Peru (9–14).
66 In addition to its sylvatic cycle, MAYV is proposed to establish urban transmission
67 through vectors such as *Aedes*, *Culex*, and *Sabethes*, with potential vertebrate reservoirs
68 including marsupials, rodents, birds, and alligators (15–17).

69 Clinically, Mayaro disease is generally a self-limiting illness characterized by fever, rash,
70 headache, photophobia, myalgia, and persistent polyarthralgia, which may last for months
71 or even years, significantly impacting patients' quality of life (18). Hemorrhagic and
72 neurological complications, as well as myocarditis, have also been reported. The clinical
73 similarity to other arboviral diseases, such as dengue and chikungunya, combined with
74 limited diagnostic capacity in endemic regions, hinders accurate differential diagnosis
75 and contributes to underestimation of the actual disease burden (18,19). Although no
76 specific antiviral treatments or licensed vaccines are currently available, several vaccine
77 candidates are under development, with sustained epidemiological surveillance
78 remaining essential to anticipate and mitigate future outbreaks (3,9,20).

79 Animal models, particularly murine species, have been instrumental in elucidating the
80 pathogenesis of Mayaro virus and in the preclinical evaluation of therapeutic and vaccine
81 candidates. These models faithfully reproduce hallmark clinical manifestations—
82 including ruffled fur, altered gait, and ocular irritation—as well as key histopathological
83 features such as arthritis, myositis, and tenosynovitis. Disease outcomes vary depending
84 on host age and immune status (21–24). The development of experimental platforms that
85 allow for robust and reproducible antiviral testing is essential for advancing MAYV
86 research. In this regard, the incorporation of *in vivo* imaging technologies represents a
87 significant methodological advancement, enabling real-time, noninvasive tracking of
88 tagged viral dissemination and host immune responses (24,25).

89 This study aims to validate and refine a murine model as a preclinical platform for future
90 evaluation of antiviral drugs and therapeutic interventions against MAYV. The model
91 incorporates *in vivo* imaging techniques, enabling real-time monitoring and longitudinal
92 analysis of viral dissemination and host response. Furthermore, the study investigates
93 viral tropism in different organs including reproductive ones, assesses the potential for

sexual transmission, and explores the possibility of vertical transmission by detecting MAYV in placenta and fetuses from infected dams, hypothesizing that MAYV infection during pregnancy results in gestational stage-dependent differences in placental permissiveness and fetal exposure. These preclinical strategies are critical to anticipate maternal and fetal health risks and to guide the development of targeted therapeutic and preventive measures.

Materials and methods

Ethics statement

All procedures and experiments were conducted in accordance with the Ethics Committee on Animal Use of the Institut Pasteur de Montevideo (CEUAIP #010-22), in compliance with National Law 18.611 "Procedures for the Use of Animals in Experimentation, Teaching, and Scientific Research Activities" and strictly followed ARRIVE guidelines.

Mice

BALB/cJ mice (#000651) were bred and maintained at the Laboratory Animal Biotechnology Unit's animal facility of Institut Pasteur de Montevideo. Mice were housed in IVC Isolator Biocontainment unit (ISOCAGE-N, Tecniplast, Milan, Italy) and acclimatized for one week prior to the experimental procedures. The cages were prepared with wood chip bedding (Toplit 6, SAFE, France), plastic tunnels as enrichment and paper napkins as nesting material. Environmental conditions were maintained at 20 ± 1°C, with 30–70% relative humidity, and a 14/10-hour light/dark cycle. The mice were provided with *ad libitum* autoclaved standard diet (D113, SAFE) and filtered, autoclaved water.

116 Mice were specific pathogen-free (SPF) certified by IDEXX (USA) quarterly, in
117 accordance with FELASA standards.

118 Experimental design

119 Although the intraplantar route more closely mimics the peripheral component of natural
120 infection, intraperitoneal (IP) inoculation was selected to ensure a standardized and
121 reproducible experimental infection. This route enables consistent systemic exposure
122 facilitating robust comparisons of viral tropism, kinetics, and systemic viral load across
123 experimental groups.

124 1) Viral tropism and health status

125 Twelve BALB/cJ female and twelve BALB/cJ male mice (4-weeks old) were IP infected
126 with $1x10^5$ PFU of MAYV Wt resuspended in 100 µL of PBS (n=24). Mock-infected
127 mice received the PBS diluent alone (n=4). Blood samples were collected for initial
128 baseline and post-infection hematological and biochemical parameter analyses at 0-, 24-
129 and 48 hpi. At 24 hpi, six animals from each sex were euthanized under deep anesthesia
130 induced by an intraperitoneal ketamine-xylazine mixture (ketamine 110 mg/kg;
131 Pharmaservice, Ripoll Vet, Montevideo, Uruguay; xylazine 13 mg/kg; Seton 2%; Calier,
132 Montevideo, Uruguay), followed by cervical dislocation for necropsy (Group 24 hpi).
133 Organs sampled for viral infectious particle counts included the liver, kidneys, spleen,
134 *quadriceps femoris* muscle, ovaries, uterus, seminal vesicles and testicles. The same
135 procedures were performed on the remaining animals 48 hpi (Group 48 hpi).

136 2) Vertical transmission

137 Fifteen BALB/cJ female mice (8-weeks old) were synchronized in their estrous cycle by
138 exposing them to male dirty bedding for 72 h prior to mating (32). Mating was then

139 performed by placing one proved male in a cage with two females for 48 h, and the
140 presence of a vaginal plug was checked daily from the following morning as a positive
141 sign of mating to be considered day 0 of pregnancy. On day 7.5-8.5 post-coitum (DPC),
142 six females were infected intraperitoneally with $1x10^5$ PFU of MAYV resuspended in
143 100 µL of PBS, while one mock-infected received only PBS diluent. The females (n=6
144 infected; n=1 mock) were euthanized 48 hpi and necropsied (9.5-10.5 DPC), and blood
145 samples were collected before euthanasia to perform hematological and biochemical
146 analyses. Organs collected for viral infectious particles count and histological analysis
147 were liver, kidneys, *quadriceps femoris* muscle, ovaries, uterus, placenta and fetus. The
148 same procedures were performed to the last eight females pregnant at 13.5-14.5 DPC
149 (n=7 infected; n=1 mock), being necropsied at 15.5-16.5 DPC.

150 **3) Sexual transmission**

151 To evaluate sexual transmission from infected female to non-infected male, seven
152 BALB/cJ female mice (8-weeks old) were synchronized in their estrous cycle by exposing
153 them to male dirty bedding for 72 h prior to mating as described above. Before mating
154 with non-infected males, the females were infected intraperitoneally with $1x10^5$ PFU of
155 MAYV resuspended in 100 µL of PBS. Infected females were euthanized and necropsied
156 48 hpi and males at 48 h after mating. Organs sampled for viral infectious particle count
157 and histological analysis included liver, spleen, *quadriceps femoris* muscle, ovaries,
158 uterus, seminal vesicles, testicles and sperm from epididymis.

159 To evaluate sexual transmission from infected males to non-infected females, six
160 BALB/cJ female mice (8-weeks old) were synchronized in their estrous cycle by exposing
161 them to male dirty bedding for 72 h prior to mating. Before mating, males were infected
162 intraperitoneally with $1x10^5$ PFU of MAYV resuspended in 100 µL of PBS. Infected

163 males were necropsied at 48 hpi and females at 48 h after mating. Organs sampled for
164 viral infectious particle count and histological analysis included liver, spleen, muscle,
165 ovaries, uterus, seminal vesicles, testicles and sperm from epididymis.

166 For analytical purposes, an exposed animal was defined as an uninfected individual mated
167 with an infected partner.

168 4) *In vivo* imaging evaluation with MAYV-nLuc infection

169 *In vivo* bioluminescence imaging was set for longitudinal monitoring of viral replication
170 over a 10-day period, capturing both acute and early recovery phases of the infection (23).
171 Age groups were selected based on previously reported differences in susceptibility to
172 Mayaro virus infection, with younger animals showing higher susceptibility(33). For this
173 study, four- and eight-week-old BALB/cJ female mice were infected intraperitoneally
174 with $1x10^4$ PFU of MAYV-Nluc resuspended in 100 µL PBS (n=4 per age group), and
175 only PBS for mock infected group (n=2, one animal per age group). To perform *in vivo*
176 luminescence imaging, the animals were injected intraperitoneally with 20 µg of
177 Furimazine (TargetMol®, MA, USA) in 100 µL of PBS, anesthetized with isoflurane and
178 imaged at different times in an In-Vivo Xtreme II™ equipment (Bruker Daltonik Gmbh,
179 Billerica, MA, USA) and analyzed using V.7.5.3.22464 MolecularImaging software
180 (Bruker Daltonik Gmbh, Billerica, MA, USA). Images were taken at 1, 2, 6 and 10 dpi.
181 Animals were necropsied at 6 dpi (n=2 animals/age group) and at 10 dpi (the remaining
182 animals). Organs sampled to confirm infectious viral particles presence included liver,
183 kidneys, spleen, *quadriceps femoris* muscle, forelimb or hindlimb and ear tissue.

184 MAYV infective clones

185 This study employed wild-type and nano Luc-expressing Mayaro virus (MAYV-nLuc)
186 infectious clones based on the TRVL 4675 strain, a genotype D virus originally isolated
187 from a human case in Trinidad in the 1950s and kindly provided by Dr. James Weger-
188 Lucarell (25–27).

189 Cell culture

190 Vero cells were maintained in in Dulbecco's Modified Eagle Medium (DMEM)
191 supplemented with 10% fetal bovine serum (FBS), penicillin (100 U/mL), and
192 streptomycin (100 µg/mL) and maintained at 37 °C, with 5% CO_2.

193 Virus generation

194 Vero cells were transfected with the TRVL 4675 infectious clone using Lipofectamine™
195 3000 Transfection Reagent (Invitrogen) to recover infectious virus. Viral supernatants
196 were collected when transfected cells exhibited an 80% cytopathic effect (CPE) and
197 stored at -70°C as passage P0.

198 To generate a working viral stock, Vero cells were infected with the P0 supernatant to
199 produce the P1 stock. Subsequently, a P2 stock was generated from P1. The P2 viral stock
200 was titrated by plaque assay, verified by sequencing and stored at -70°C until further use.

201 Infectious virus was rescued from both WT and MAYV-nLuc infectious clones by
202 transfection of Vero cells using Lipofectamine™ 3000 (Invitrogen), according to the
203 manufacturer's instructions. Viral supernatants were collected when transfected cells
204 exhibited an 80% cytopathic effect (CPE) and stored at -70°C as passage P0.

205 Working viral stocks were generated by sequential infection of Vero cells to produce P1
206 and P2 passages. The P2 viral stocks were titrated by plaque assay, verified by sequencing
207 and stored at -70°C until further use.

208 ## Hematology and biochemistry profile

209 For hematological analysis, 20 µL of blood per animal were collected and stored in 0.5
210 mL microtubes containing potassium EDTA salts (W anticoagulant, Wiener Lab,
211 Rosario, Argentina) at a 1:10 ratio (EDTA: blood). Samples were analyzed using an Auto
212 Hematology Analyzer BC-5000 Vet (Mindray, Shenzhen, China). The parameters
213 evaluated included white blood cells (WBC), neutrophils (Neu), lymphocytes (Lym),
214 monocytes (Mon), eosinophils (Eos), basophils (Bas), red blood cells (RBC), hemoglobin
215 (HGB), hematocrit (HCT), mean corpuscular volume (MCV) and mean corpuscular
216 hemoglobin (MCH), mean corpuscular hemoglobin concentration (MCHC) and platelets
217 (PLT).

218 For biochemical blood profile analysis, 100 µL of whole blood per animal was collected
219 and mixed with 0,5 µL of sodium heparin (Heparin Na, 20 U/mL). Using the Chemistry
220 Analyzer Pointcare® V3 (Tianjin MNCHIP Technologies Co. Ltd, Tianjin, China), the
221 following parameters were evaluated: total protein (TP), albumin (ALB), globulin (GLO),
222 total bilirubin (Tbil), alanine aminotransferase (ALT), aspartate aminotransferase (AST),
223 gamma-glutamyl transferase (GGT), blood urea nitrogen (BUN), and creatinine (CRE).

224 In pregnant infected females, hematological analysis was performed at early and mid-
225 gestation stages 48 hours post-infection (hpi), using samples collected exclusively at
226 necropsy, without pre-infection baseline values.

227 ## Tissue collection and processing

228 Samples collected from each organ of interest were weighed, rapidly frozen in liquid
229 nitrogen under a biosafety cabinet and stored at -70°C until processing. Samples were
230 homogenized using zirconium beads (0.5 mm/tube) and 800 µL of sterile 1× DPBS in a

231 Precellys® 24 homogenizer (Bertin Technologies, France), (2 min, power 10).
232 Homogenates were clarified by centrifugation (6,000 × g, 5 min), and supernatants were
233 stored at −70 °C for viral titration or RT-qPCR analysis

234 Viral titration

235 For viral titration, confluent Vero cell monolayers in 12-well plates (2.6×10^6 cells per
236 plate) were inoculated with tissue homogenate–derived supernatants and their 10-fold
237 serial dilutions (200 µL per well) and incubated at 37 °C with 5% CO_2 for 1 h, with gentle
238 rocking every 15 min to ensure uniform inoculum distribution. Mock-infected wells
239 served as negative controls. The monolayer was incubated at 37°C with 5% CO_2 for 1 h,
240 with gentle shaking of the plate every 15 minutes to ensure the inoculum contacted the
241 entire monolayer. After adsorption, cells were overlaid with DMEM containing 0.8%
242 agarose, 1.6% FBS, penicillin, and streptomycin and incubated for 48 h. Monolayers were
243 then fixed with 4% formaldehyde, stained with crystal violet, and plaques were counted
244 to determine viral titers, expressed as plaque-forming units per gram of tissue (PFU/g).

245 Mouse sperm collection

246 The epididymides from both sides were collected in a 60 mm plastic Petri dish and incised
247 with several cuts using fine scissors, releasing the sperm into a 50 µL drop of Dulbecco's
248 Phosphate Buffered Saline 1x (DPBS, Sigma-Aldrich), and stored at −80°C until further
249 processing. Later, sperm samples were thawed and resuspended in 150µL of PBS.
250 Zirconium beads were added to each sample and disruption was performed using a Bullet
251 Blender® STORM 24 (Next Advance Inc., New York, USA) during one minute at speed
252 8. After centrifugation, 100µL of supernatant were removed for cell culture–based viral
253 amplification and viral ARN detection.

254 # Viral RNA extraction and detection

255 Viral RNA from tissues was purified from clarified supernatants obtained after tissue
256 homogenization, as described above, using the QIAamp® Viral RNA Mini Kit
257 (QIAGEN), according to the manufacturer's instructions. RNA from sperm samples was
258 extracted from TRIzol-treated homogenates using the Direct-zol RNA Miniprep Kit
259 (Zymo Research), following the manufacturer's guidelines. RNA samples were eluted in
260 25µL of nuclease-free water and conserved at -70ºC until further use (28).

261 Detection was performed using a one-step real-time reverse transcription PCR (RT-
262 qPCR) assay, employing the primers and probe listed in Table 1, which target an 86-bp
263 region of the MAYV nsP1 gene. Reactions were carried out using TaqMan™ Fast Virus
264 1-Step Master Mix (Thermo Fisher Scientific) on a QuantStudio™ 7 Pro Real-Time PCR
265 System (Applied Biosystems). Due to limited sample availability, sperm-derived RNA
266 samples were analyzed in technical duplicates. The assay was used for qualitative
267 detection (presence/absence) of viral RNA.

268 **Table 1: primers and probe used for MAYV detection by qPCR.**

MAY-qPCR-Fw	AGGACCCAGAGGAACACTAATA
MAY-qPCR-Rv	CGATACTCTTTCGCCCACTTAC
MAY-qPCR-Probe	/56-FAM/TACCTGCTT/ZEN/CCAGTGGTGTCACAA/3IABkFQ/

269

270 # Cell culture–based isolation of virus from sperm samples

271 Due to the limited volume of sperm samples, processed samples were subjected to
272 passage in Vero cells to allow potential biological amplification prior to titration. Vero
273 cells were seeded in 96-well plates at 5,000 cells per well in 100 µL of DMEM

274 supplemented with 5% FBS, penicillin (100 U/mL), and streptomycin (100 µg/mL). The
275 following day, cells were inoculated with 100 µL of processed sperm samples. Mock-
276 infected wells receiving culture DMEM alone served as negative controls. After 72 h of
277 incubation at 37 ºC, supernatants were harvested and the presence of infectious viral
278 particles was assessed by plaque assay. Cytopathic effects were monitored using inverted
279 optic microscope Zeiss Primovert, Carl Zeiss Suzhou Co., LTD, China.

280 Transcriptomics in placenta

281 For the RNA-seq experiment, three placentas per condition (control uninfected; infected
282 at 7.5-8.5 DPC; infected at 13.5-14.5 DPC) were selected and processed for total RNA
283 extraction. Placentas stored at −80 °C were disrupted in TRI Reagent using a Bullet
284 Blender® STORM 24 (Next Advance Inc., New York, USA) with 0.5 mm zirconium
285 oxide beads (ZROB05, Next Advance Inc.) for 10 min at maximum speed. Following
286 homogenization, the samples were centrifuged to remove beads and debris. The upper
287 aqueous phase was collected and purified using the Direct-zol RNA kit (Zymo Research,
288 USA) according to the manufacturer's instructions. RNA was quantified with RNA HS
289 Qubit (Invitrogen, USA). RNA quality check, library construction and sequencing were
290 performed in Macrogen (Korea). TruSeq stranded total RNA with Ribo-Zero Gold
291 (Illumina, USA) platform was used. Sequencing was performed in the Illumina
292 NovaSeqX. Paired-end reads of 100 base pairs were obtained.

293 Raw paired-end RNA-seq reads were aligned to the *Mus musculus* reference genome
294 (GRCm39, Ensembl release 114) using STAR v2.7.8a. Aligned reads were quantified at
295 the gene level using featureCounts v2.0.2 (Subread package). The Ensembl GTF
296 annotation file (Mus_musculus.GRCm39.114.gtf) was used.

297 Downstream analysis was conducted in R v4.3.0 using the DESeq2 package. The raw
298 count matrix was filtered to retain genes with a minimum of 10 total reads across all
299 samples. A DESeq2 dataset was constructed with experimental conditions as the main
300 design factor. Variance stabilizing transformation (VST) was applied to normalize data
301 prior to visualization and clustering. Differential expression analyses were performed for
302 multiple contrasts of interest, and log2 fold changes were shrinkage-corrected using the
303 "normal" method of lfcShrink. Genes with an adjusted p-value <0.05 were considered
304 significantly differentially expressed.

305 Volcano plots were generated with ggplot2, where significant genes were highlighted
306 (adjusted p <0.05). Heatmaps of differentially expressed genes were created with
307 pheatmap R package, using variance-stabilized expression values scaled by gene (row-
308 wise z- scores). Color schemes were defined with the RColorBrewer package. Additional
309 2 hierarchical clustering of differentially expressed genes was performed to assess global
310 expression patterns across experimental groups. Gene ontology analysis was performed
311 using Metascape (29)

312 Immunohistochemistry

313 Immediately after the necropsy, placenta and fetus from mid-stage of pregnancy were
314 fixed in 10% neutral buffered formalin (pH 7.4) for further processing. The samples were
315 then decalcified by immersion and agitation in a 3% aqueous nitric acid solution for 24
316 h. Once decalcification was complete, histological processing for paraffin embedding
317 began. Once the paraffin blocks were obtained from each sample, successive 4µm-thick
318 sections were made with a manual rotary microtome (Slee, Germany), and the successive
319 sections were mounted on slides and prepared for immunohistochemistry against Mayaro
320 virus immunoreaction, using a rabbit polyclonal primary antibody (dilution 1:100)

321 according to a previous immunofluorescence protocol developed for
322 immunocytochemistry in cell cultures (30,31). Histological and immunohistochemical
323 blinded examinations were performed using transmitted light microscope (Nikon Eclipse
324 E200®, Nikon Corporation, China) by two different veterinary pathologists.

325 Data Analysis

326 All data were analyzed using GraphPad Prism version 10 (GraphPad Software, San
327 Diego, CA, USA). Two-way analysis of variance (ANOVA) or mixed-effects analysis,
328 followed by Tukey's multiple comparisons test, was applied to evaluate differences
329 among viral titers across tissues and blood parameters. Paired comparisons between pre-
330 and post-infection values were performed using Student's t-test. Results were expressed
331 as mean ± standard error of the mean (SEM), and differences were considered statistically
332 significant when $p < 0.05$.

333

334 Results

335 Viral tropism and health status

336 MAYV rapidly disseminates to somatic and reproductive tissues during
337 acute infection

338 Viral titration by plaque assay revealed widespread MAYV dissemination across multiple
339 organs at early time points post-infection in both sexes. Infectious viral particles were
340 also detected in reproductive organs: uterus, ovary, seminal vesicles and testicles (Fig
341 1A). At 24 hpi (Group 24 hpi), the virus exhibited a widespread systemic distribution,

342 with detectable viral titers across most of the analyzed organs. Although higher values
343 were observed in the spleen and muscle, no statistically significant differences were found
344 among organs, indicating an early but relatively homogeneous viral dissemination at this
345 stage. At 48 hpi (Group 48 hpi), infectious viral loads were significantly higher in the
346 spleen compared to kidneys (p = 0.0122) and muscle (p = 0.0164), reaching ~3.5 × 10^6
347 PFU/g. At 24 hpi, sex-based analysis showed that females hosted lower viral titers than
348 males in spleen (p = 0.0038) and muscle (p = 0.0286), while no differences were detected
349 in liver or kidneys (Fig 1B). At 48 hpi, these sex-related differences were no longer
350 observed. However, in females, spleen viral loads were higher than in kidneys (p =
351 0.0181) and muscle (p = 0.0105), whereas inter-organ differences were not significant in
352 males (Fig 1C).

FIGURE 1

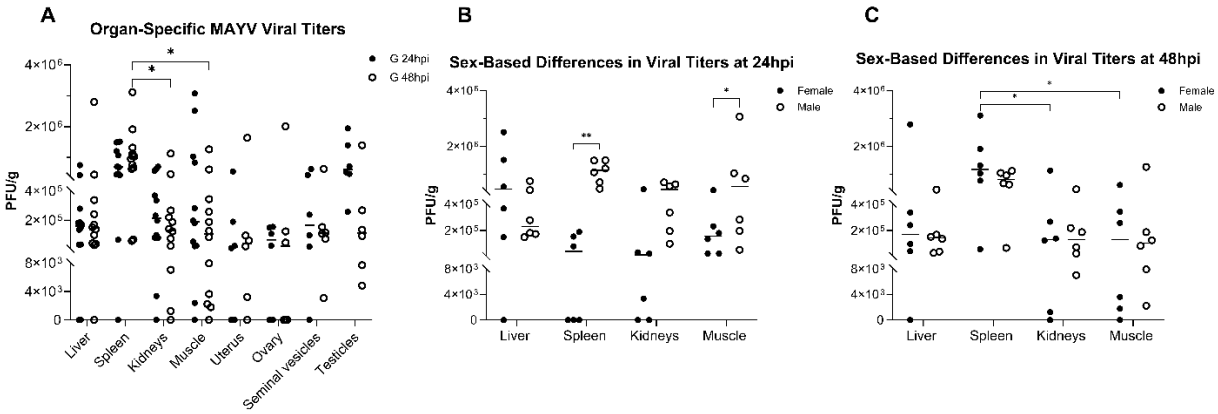

353

354 **Fig 1. MAYV viral titration in male and female mouse tissues.** A) Viral loads (PFU/g)
355 were quantified by plaque assay at 24 and 48 hpi in kidney, liver, spleen, muscle, uterus,
356 ovary, seminal vesicles and testicles. B) and C) Viral titers in male and female mice at 24
357 hpi (B) and 48 hpi (C). Two-way ANOVA followed by Tukey's multiple comparisons
358 test was performed. Statistical significance was defined as $p < 0.05$ (*) and $p < 0.01$ (**).

359 **Acute MAYV infection induces transient hepatic and renal biochemical**

360 **alterations**

361 Early infection was associated with transient alterations in blood biochemistry. Total
362 protein levels declined 48 hpi (Fig 2 A, p = 0.0001), total bilirubin decreased at 24 hpi
363 and in mock infected animals also (Fig 2B), while hepatic enzymes showed evidence of
364 liver damage, with ALT (Group 48 hpi) and AST (Group 24 hpi and Group 48 hpi)
365 increasing after infection (Fig 2 C and D respectively, p = 0.0142; p <0.0001 and p =
366 0.0021). In contrast, GGT remained unchanged (Fig 3A). Kidney parameters displayed a
367 mixed profile: blood urea nitrogen (BUN) levels decreased 24 hpi (Fig 3B, p = <0.0001)
368 while creatinine showed no differences 24 or 48 hpi, with higher values in infected groups
369 (Fig 3C).

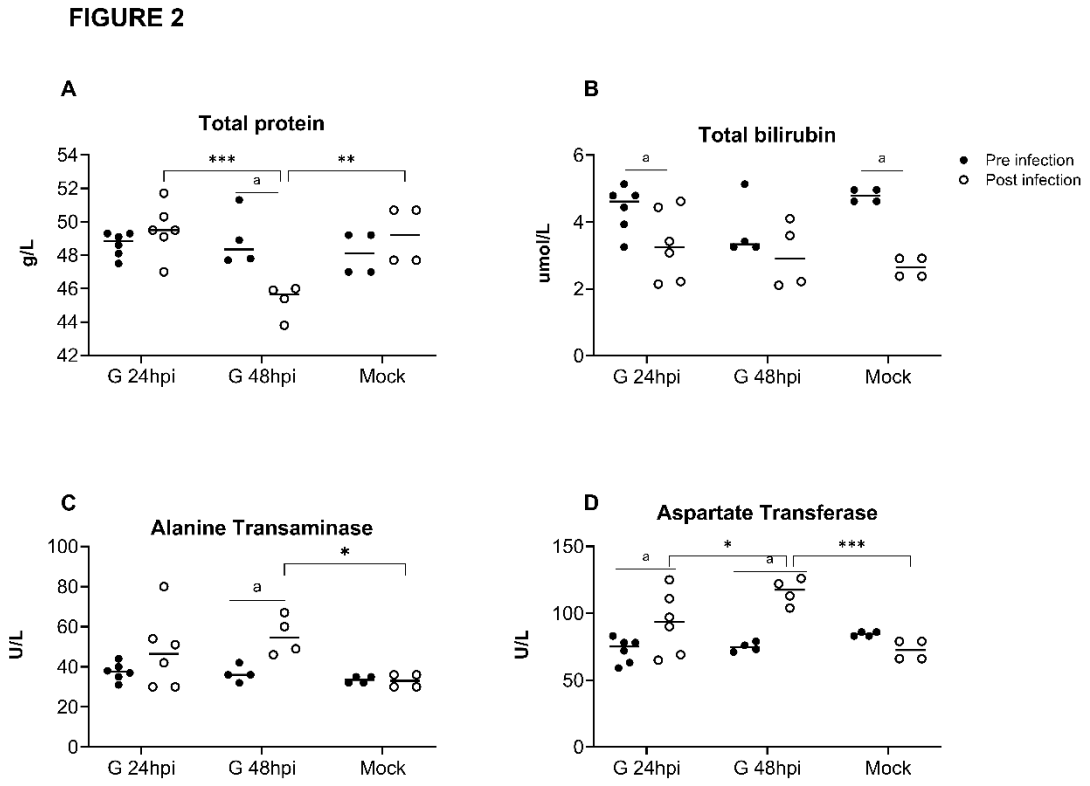

370

371 **Fig 2. Blood biochemical parameters pre and post MAYV infection.** (A) Total protein,
372 (B) Total bilirubin, (C) Alanine transaminase (ALT), and (D) Aspartate transferase (AST)

373 levels in blood samples of infected and mock-treated animals at 0, 24 and 48 hpi. Each
374 dot represents an individual animal; horizontal lines indicate median values. Black circles
375 = pre-infection; open circles = post-infection. Statistical significance was determined
376 using a Mixed-effects analysis followed by Tukey's multiple comparisons test.
377 Differences among treatments were considered significant at $p < 0.05$ (*), $p < 0.01$ (**),
378 and $p < 0.001$ (***). Pre- versus post-infection comparisons were considered significant
379 at $p < 0.05$ (a).

FIGURE 3

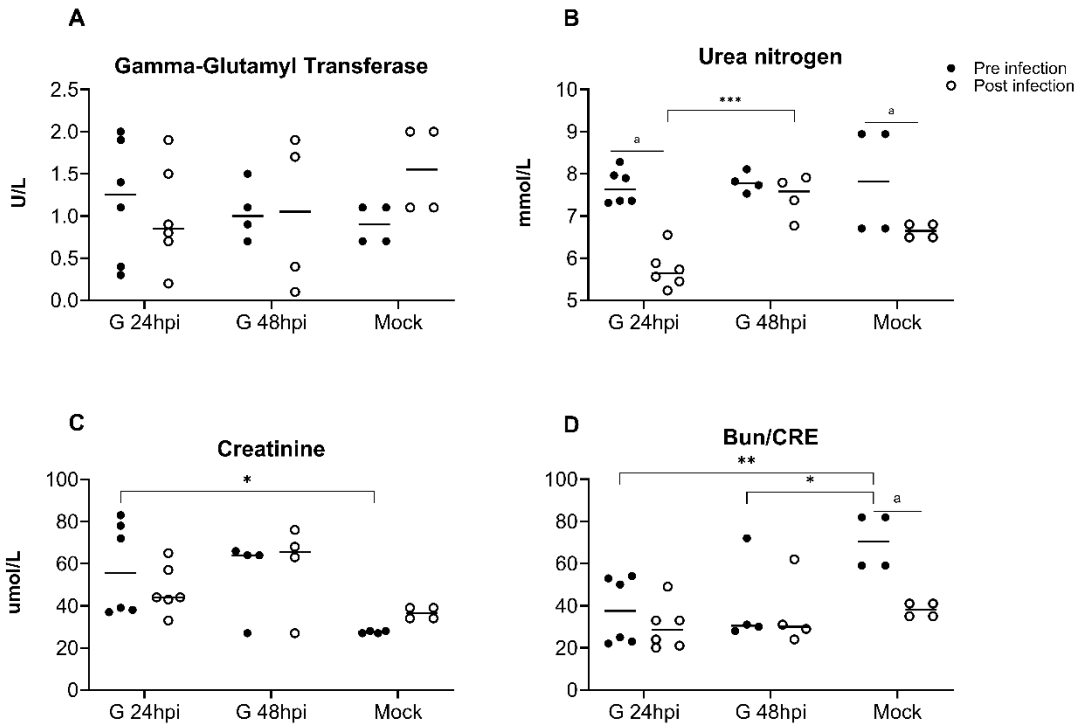

380

381 **Fig 3. Kidney blood markers pre and post MAYV infection.** (A) Gamma-glutamyl
382 transferase (GGT), (B) blood urea nitrogen (BUN), (C) creatinine, and (D) BUN/CRE
383 ratio in serum 24 and 48 hpi compared to mock treated animals. Each dot represents an
384 individual animal; horizontal lines indicate median values. Statistical significance was
385 determined using a Mixed-effects analysis followed by Tukey's multiple comparisons
386 test. Differences among treatments were considered significant at $p < 0.05$ (*), $p < 0.01$

387 (**), and $p < 0.001$ (***). Pre- versus post-infection comparisons were considered
388 significant at $p < 0.05$ (a).

389 MAYV infection induces hematological alterations consistent with 390 systemic viral disease

391 Hematological analysis of infected mice showed leukopenia, neutrophilia, lymphopenia,
392 thrombocytopenia and transient macrocytosis in both groups (24 and 48 hpi) (Fig 4; S1
393 and S2 Figs). White blood cells count and lymphocyte % were significantly reduced in
394 both groups after infection ($p < 0.0001$), with an increase in neutrophils ($p < 0.05$),
395 decrease in monocytes and eosinophils count ($p < 0.05$), and basophils % increased only
396 48 hpi ($p < 0.05$). Erythrocyte parameters showed higher red blood cell (RBC) counts 48
397 hpi ($p < 0.05$), plus hemoglobin and hematocrit increased in both groups ($p < 0.05$) (S3
398 Fig), with associated increases in Mean Corpuscular Volume (MCV) and Mean
399 Corpuscular Hemoglobin (MCH) while Mean Corpuscular Hemoglobin Concentration
400 (MCHC) remained stable (S4 Fig). Platelet counts and Procalcitonin decreased in both
401 groups ($p < 0.05$) (S5 Fig).

FIGURE 4

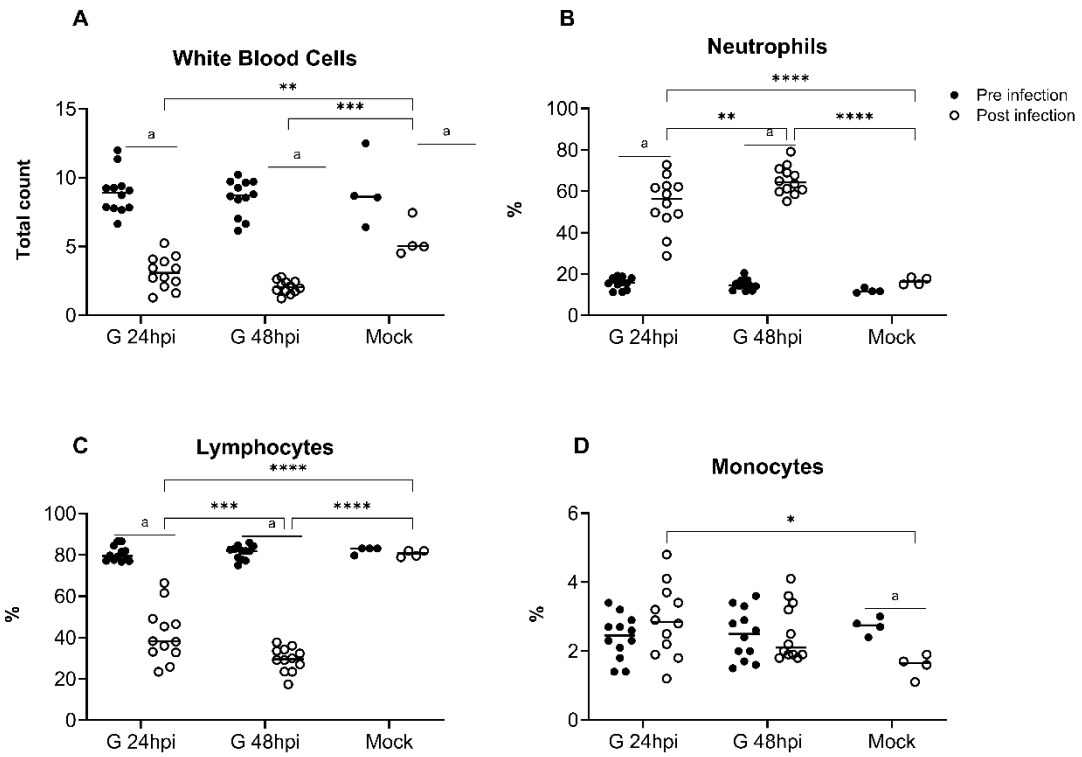

Fig 4. White blood cell dynamics pre- and post- MAYV infection. A) Total white blood cell count, B) Percentage of neutrophils, C) Percentage of lymphocytes, and D) Percentage of monocytes. Each dot represents an individual animal; horizontal lines indicate median values. Black circles = pre-infection; open circles = post-infection. Statistical significance was determined using a Mixed-effects analysis followed by Tukey's multiple comparisons test. Differences among treatments were considered significant at $p < 0.05$ (*), $p < 0.01$ (**), and $p < 0.001$ (***). Pre- versus post-infection comparisons were considered significant at $p < 0.05$ (a).

Vertical transmission

Gestational stage determines placental permissiveness and fetal exposure to MAYV

414 In females infected at 7.5–8.5 DPC (early stage of pregnancy), infective viral particles
415 were detected in all the analyzed organs except for liver and kidneys, with higher titers
416 observed in spleen ($p < 0.0114$), uterus ($p < 0.0111$), fetuses ($p < 0.0016$) and placenta (p
417 < 0.0012) compared to muscle (Fig 5).

418 For females infected at 13.5–14.5 DPC (mid-stage pregnancy), viral titers were broadly
419 distributed across the analyzed organs except in fetuses, with no statistically significant
420 differences among them (Fig 5).

421 When comparing females infected at early versus mid gestation, viral titers were
422 significantly higher at mid stage in the uterus ($p < 0.0268$) and muscle ($p < 0.0004$). All
423 results are shown in Fig 5.

424

FIGURE 5

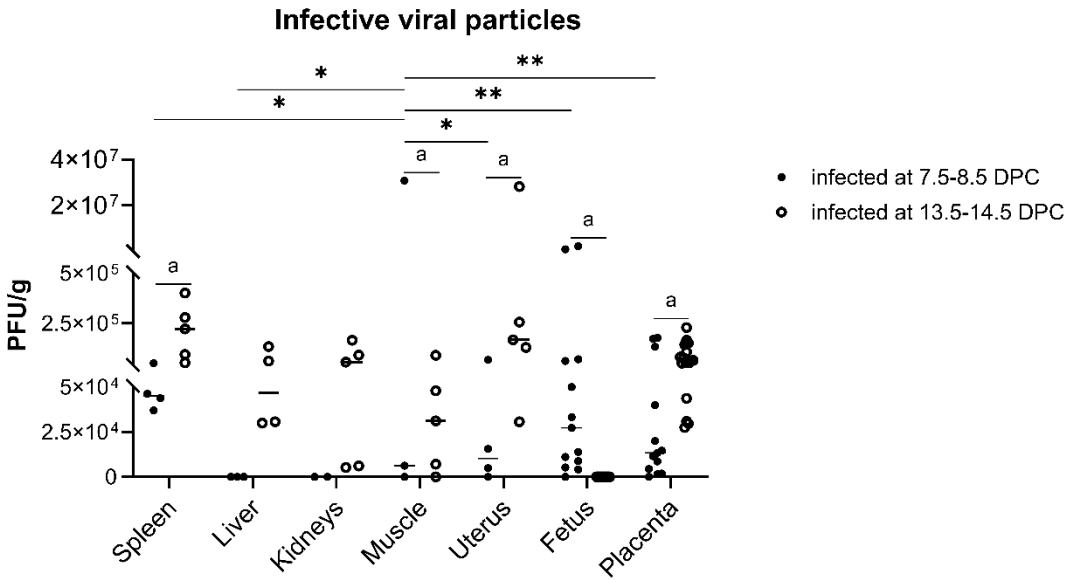

425

426 **Fig 5. Infective viral particles in organs of early and mid-stage pregnant females 48**
427 **hpi.** Quantification of infective viral particles (PFU/g) in maternal and fetal tissues from
428 females infected at early (●: 7.5–8.5 DPC) and mid (○: 13.5–14.5 DPC) gestational

429 stages. Data are expressed as individual values with mean lines. Statistical significance
430 was determined using a Mixed-effects analysis followed by Tukey's multiple
431 comparisons test. Differences among treatments were considered significant at $p < 0.05$
432 (*), $p < 0.01$ (**), and $p < 0.001$ (***) among groups. Comparisons were considered
433 significant at $p < 0.05$ (a) between groups ((7.5–8.5 vs13.5–14.5 DPC).

434 Pregnancy-associated MAYV infection alters leukocyte dynamics 435 without overt hematological collapse

436 Infected females at both gestational stages showed neutrophilia and lymphopenia;
437 significantly higher neutrophil percentages compared to their respective controls ($p <$
438 0.05), and a corresponding decrease in lymphocyte percentages ($p < 0.05$). Red blood cell
439 counts remained similar between infected and control groups. Although a decrease in
440 parameter levels was observed, no significant differences were found in total white blood
441 cell counts, platelet counts, or procalcitonin levels between infected and mock females at
442 either gestational stage (S6 and S7 Figs).

443 Immunohistochemistry confirms placental and fetal localization of 444 MAYV at mid stage

445 Immunohistochemical detection of MAYV in fetus and placenta from an infected female
446 at 13.5–14.5 DPC revealed distinct staining patterns between infected and non-infected
447 controls. In placentas from infected females, moderate granular cytoplasmic staining was
448 observed, marking a substantial proportion of the giant trophoblast cells within the
449 maternal–fetal junction zone (basal plate). In contrast, placentas from non-infected
450 pregnant females showed only nonspecific erythrocyte staining and overall negative to
451 mild background labeling. In fetus from infected female, intense immunostaining was

452 detected across multiple organs, particularly in the visceral epithelium of the intestine,
453 the developing bone (growth cartilage), and other collagen-rich tissues including cartilage
454 and dermis. Calcified bone exhibited no staining or only minimal labeling in both
455 intensity and extent. Fetuses from non-infected females displayed only nonspecific
456 erythrocyte staining, generally negative overall, with minimal background labeling in
457 collagen-rich tissues (Fig 6).

FIGURE 6

458 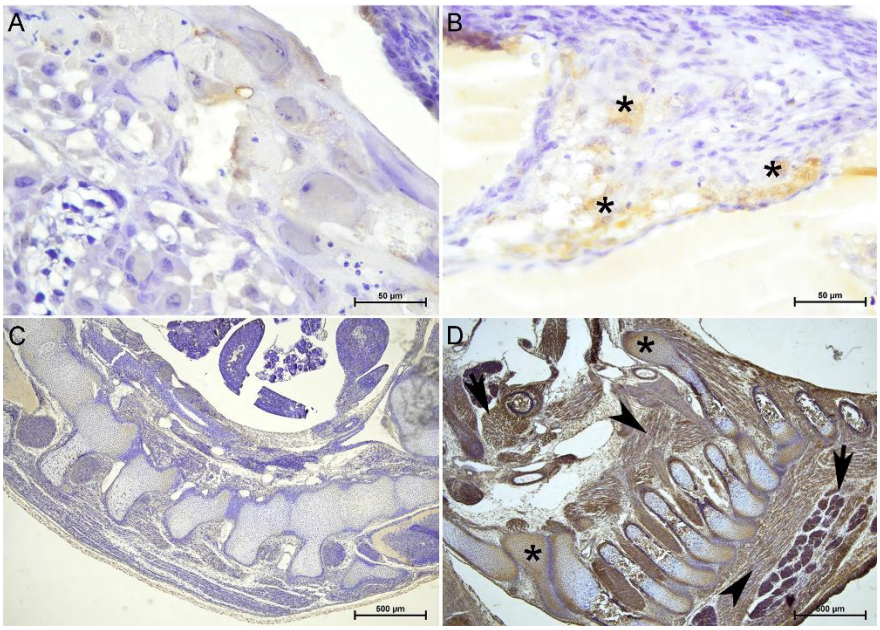

459 **Fig 6. IHC against Mayaro virus**. A) Placenta of an uninfected mouse (control):
460 Negative to mild (-/+) immunostaining of isolated trophoblasts (foam giant cells) from
461 the basal plate of the maternal-fetal junction is observed. Scale bar = 50µm, 40×. B)
462 Placenta of an experimentally infected mouse: Mild to moderate, granular
463 intracytoplasmic staining of foci of trophoblasts (foam giant cells) from the basal plate of
464 the maternal-fetal junction is observed (asterisks). Scale bar = 50µm, 40×. C) Fetus of the
465 same uninfected mouse of Fig A: No immunostaining against Mayaro virus is observed
466 (-). Scale bar = 500µm, 4×. D) Fetus of the same experimentally infected mouse of Fig
467 B: There is intense immunostaining in several organs, particularly in uncalcified

468 developing bone and growth cartilage (asterisks), as well as other collagen-rich tissues
469 (cartilage and dermis) (arrowheads) and the perimysium of skeletal muscles (arrows).
470 Already calcified bone shows no staining or minimal staining in intensity and extent.
471 Scale bar = 500μm, 4×.

472 Placental transcriptional responses to MAYV are gestational stage-
473 dependent

474 Differential gene expression of placentas infected at 7.5–8.5 DPC (early stage) versus
475 control, and 13.5–14.5 DPC (mid-stage) versus control were performed, and patterns of
476 expression compared. The profiles revealed gene expression patterns influenced by viral
477 infection at early and mid-stages: 208 genes were upregulated and 60 downregulated at
478 the early stage, and 139 genes were upregulated and 1 downregulated at the mid stage
479 (Fig 7A, S1 Table). Among the upregulated genes, 50 were shared between both stages,
480 leaving 158 stage-specific upregulated genes at the early stage and 89 at the mid stage.
481 These data suggest a robust transcriptional response to infection during the early stage of
482 pregnancy, while the response in mid pregnancy, although sharing common pathways, is
483 comparatively attenuated.

484 Gene Ontology (GO) enrichment analysis of the 50 shared upregulated genes revealed
485 their significant association with pathways related to response to viral infection,
486 modulation of host responses by interferon-stimulated genes (ISGs), and positive
487 regulation of cytokine-mediated signaling (Fig 7B). The 158 genes uniquely upregulated
488 in the early stage were enriched not only for the immune pathways but also for distinct
489 biological processes, including heart development, myeloid cell development, regulation
490 of plasminogen activation, connective tissue development, and adipogenesis (Fig 7C). In
491 contrast, the 89 late-stage-specific upregulated genes were again predominantly

492 associated with immune functions, specifically type II interferon signaling, negative
493 regulation of innate immune response, and innate antiviral immune response (Fig 7D).
494 Furthermore, GO analysis of the 60 genes downregulated specifically at the early stage
495 identified enrichment for processes such as multi-organism reproductive process, antigen
496 processing and presentation of peptide antigen via MHC class I, lymphocyte activation,
497 signaling by NTRKs, insulin secretion, thermogenesis, extracellular matrix organization,
498 and adrenergic signaling in cardiomyocytes (Fig 7E).

FIGURE 7

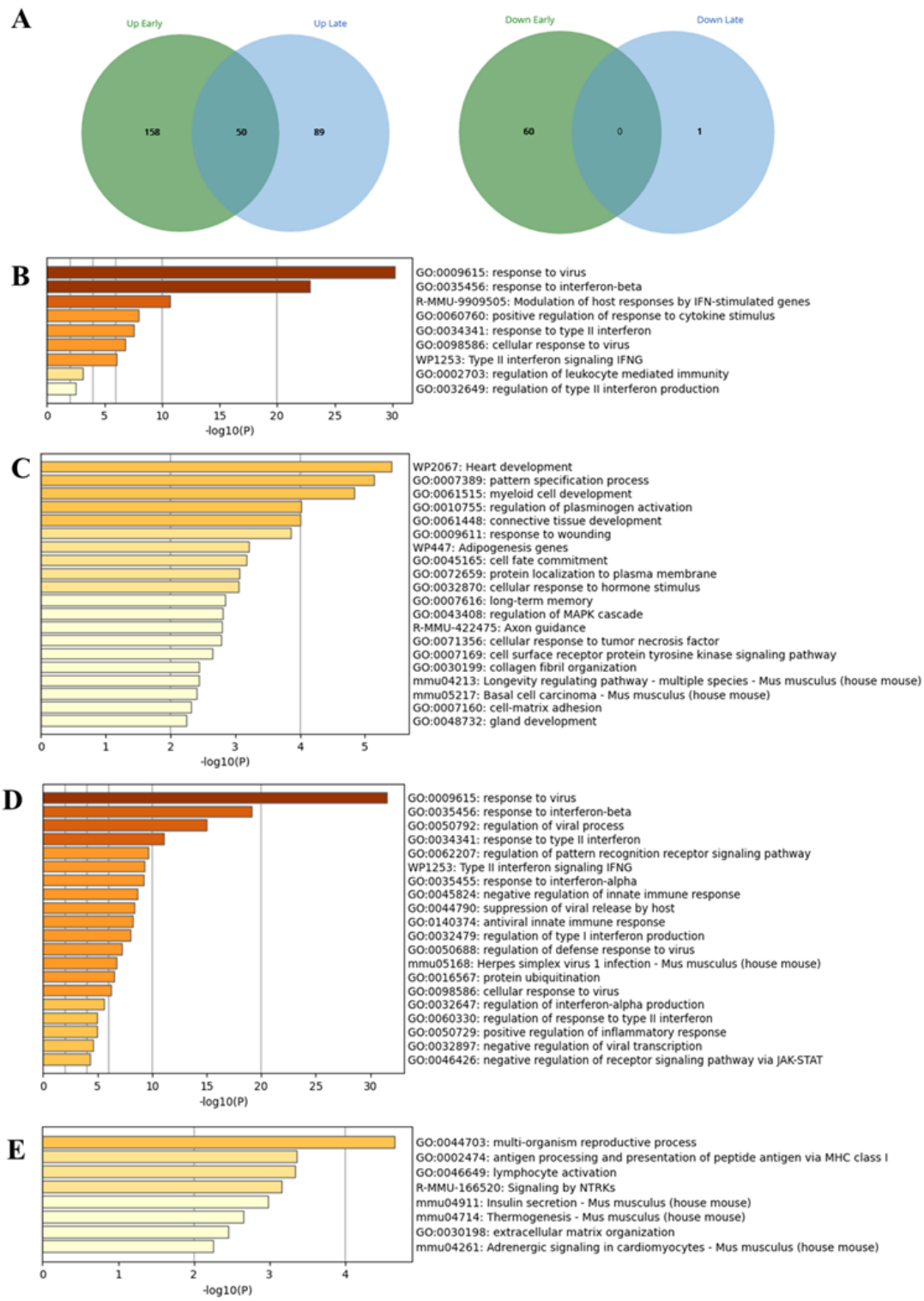

Fig 7. Transcriptomic profiles and Gene Ontology enrichment of placental response to MAYV infection at early and mid-gestational stages. A) Comparison of placentas

502 infected at 7.5–8.5 DPC (early) and 13.5–14.5 DPC (late) versus controls revealed 208
503 up-/60 down-regulated genes at early stage and 139 up-/1 down-regulated at mid stage,
504 with 50 genes shared between stages. B) Shared genes were enriched for antiviral and
505 interferon-mediated responses. C) Early-stage-specific genes were associated with
506 immune, developmental, and metabolic pathways. D) Late-stage-specific genes were
507 mainly related to type II interferon and innate immune modulation. E) Early-stage down-
508 regulated genes were enriched for reproductive, metabolic, and signaling processes.

509 # Sexual transmission

510 ## Reproductive tissue tropism and detection of MAYV in sperm support
511 ## the possibility of sexual transmission.

512 Infective viral particles were detected in the spleen (7/7), ovary (3/7) and muscle (1/7) of
513 infected females (n = 7) mated with uninfected males. In contrast, all organs analyzed
514 from exposed males tested negative by plaque assay and RT-qPCR. However, following
515 cell culture-based amplification of sperm samples, infectious viral particles in one male
516 (1/7), which had been paired with the female positive for infectious virus in both spleen
517 and muscle.

518 In infected males (n = 6) mated with uninfected females, infective particles were
519 consistently detected in testicles (6/6) and, to a lesser extent, in spleen (3/6). Moreover,
520 cell culture-amplified sperm samples were positive for infectious virus in four males (4/6;
521 Fig 8), and viral RNA was detected by RT-qPCR in sperm samples from the same four
522 animales.). No infectious virus was detected in seminal vesicles from adult males.

523 Among exposed females, infectious viral particles were detected in two animals: uterus
524 and ovary of one female, and in the spleen of another. In both cases, viral titers were low

525 by plaque assay and not reproducible upon repeat testing. Consistently, viral RNA levels
526 in these samples were below the limit of detection by RT-qPCR.

FIGURE 8

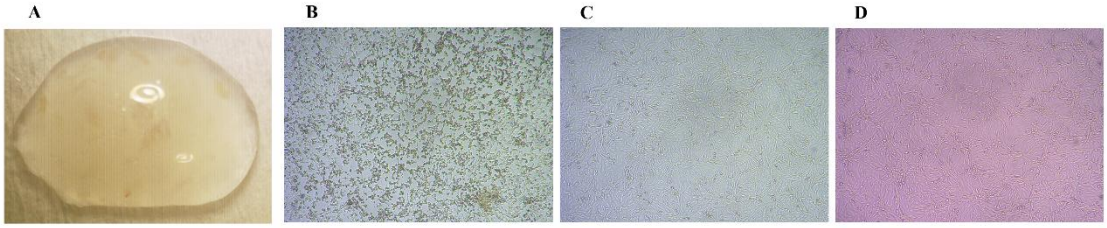

527

528 **Fig 8. Detection of infectious MAYV in sperm samples following cell culture–based**
529 **amplification.** (A) Sperm extracted from the epididymis. (B; D) Representative images
530 of Vero cells inoculated with processed sperm samples showing a MAYV-positive
531 sample (B) a MAYV-negative sample (C) and Mock-infected Vero cells (D). Images were
532 acquired using a Zeiss Primovert inverted light microscope (40×).

533 *In vivo* **imaging**

534 **Bioluminescence imaging reveals rapid dissemination and**
535 **musculoskeletal persistence of MAYV**

536 MAYV-nLuc viral dissemination was detectable in inoculated mice as early as 24 hpi and
537 remained up to 10 days post-infection (dpi). *In vivo* bioluminescence imaging revealed
538 viral signaling in forelimbs, hindlimbs, tails, ears, and abdominal region. The abdominal
539 signal progressively declined after 6 dpi. Luminescence in limbs, tail, and ears persisted,
540 with signal remaining detectable only in the limbs at 10 dpi (Fig 9). *Ex vivo* plaque assays
541 were performed on harvested tissues. Infectious viral particles were detected in forelimbs,
542 hindlimbs, tail, and ears of 4-week-old mice, whereas visceral organs (liver, spleen,

skeletal muscle, and kidneys) yielded negative results. Tissues from 8-week-old animals that retained luminescent signals *in vivo* were negative by plaque assay.

FIGURE 9

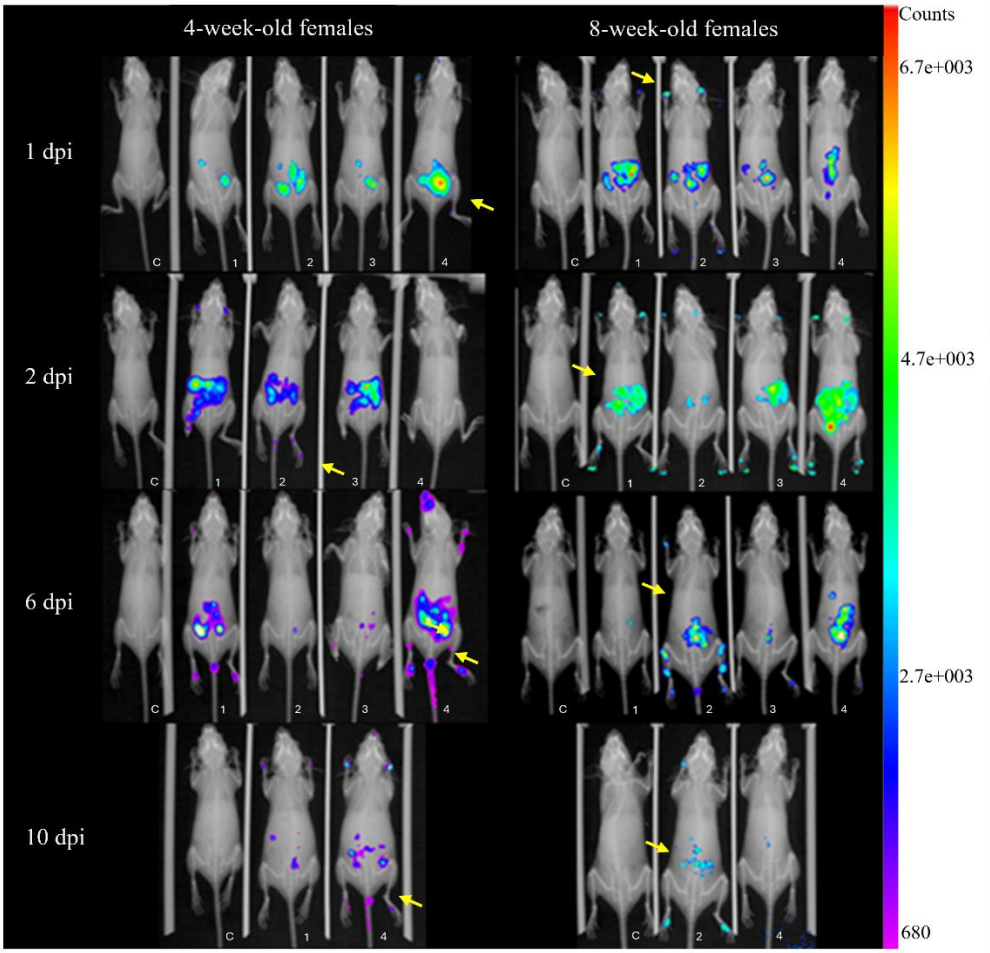

Fig 9. Representative images of *in vivo* bioluminescence imaging of MAYV-nLuc infection in females at 4 and 8 weeks-old. Luminescent signals (yellow arrows) were detected in the limbs, tail, ears, and abdominal region from 1 up to 10 dpi with the abdominal signal declining after 6 dpi.

Discussion

Elucidating the tissue tropism and viral dynamics of Mayaro virus (MAYV) is essential given the limited evidence available for this emerging arbovirus and the relevance of

553 murine models for characterizing infection *in vivo*. Here, we provide the first evidence of
554 MAYV dissemination to fetal tissues in mice, identifying anatomical targets not
555 previously described. Together, these findings support a model in which gestational
556 timing critically determines placental permissiveness and fetal exposure to MAYV,
557 identifying early gestation as a window of heightened vulnerability during acute infection.
558 Considering that related alphaviruses can cross the placental barrier, our results
559 underscore the importance of including pregnancy models when assessing MAYV
560 transmission routes.

561 MAYV exhibited rapid and systemic dissemination at 24 and 48 hpi, with infectious virus
562 detected across multiple organs, including detection in reproductive tissues of pregnant
563 females. These results are consistent with other murine alphavirus models, including
564 IFNAR−/− mice, in which widespread viral detection at early time points reflects acute
565 viremia (24). Infectious viral loads were significantly higher in the spleen at 48 hpi, in
566 agreement with its role as a primary replication site ; (10,34) , and infectious particles
567 were also found in muscle, supporting previously described myopathy and myositis
568 associated with MAYV infection (10,35).

569 Biochemical analysis revealed elevated in ALT and AST levels, consistent with hepatic
570 injury described in both murine and human MAYV infection (18,23). Hematological
571 alterations, including macrocytosis, leukopenia, neutrophilia, and lymphopenia, mirrored
572 previous reports in murine models (23,24) and human cases (18). Together, these
573 systemic responses further validate the relevance of this murine model for studying
574 MAYV pathogenesis.

575 MAYV belongs to the Alphavirus genus (18,36) , which includes viruses capable of
576 affecting the nervous system and embryonic development. The detection of infectious

577 particles in reproductive organs (uterus, ovary, testes, seminal vesicles) at both time
578 points highlights a tissue tropism previously described in immunodeficient mice (15) and
579 raises the possibility of sexual or vertical transmission. Sex-based differences were
580 observed during acute infection: with females displaying lower viral titers than males in
581 the spleen and muscle at 24 hpi. These differences were no longer evident at 48 hpi. While
582 most studies focused on age and nutritional status as determinants of disease outcome ; ;
583 (23,25,37), these observations suggest a potential sex-dependent component of MAYV
584 infection that warrants further investigation, particularly given similar findings reported
585 for Chikungunya virus (38).

586 A gestational stage–dependent susceptibility was evident. At early pregnancy (7.5–8.5
587 DPC), fetuses contained infectious particles at 48 hpi, indicating that MAYV can cross
588 the maternal–fetal barrier during acute infection. This window—analogous to early
589 human embryogenesis (39) displayed a broad transcriptional response (208 upregulated,
590 60 downregulated genes), including alterations in developmental and tissue-remodeling
591 programs, as well as downregulation of hormonal signaling, MHC I presentation, and
592 ECM organization. These disruptions are compatible with teratogenesis described for
593 alphaviruses such as Semliki Forest virus (37) and ZIKV (40).

594 In contrast, at mid gestation (13.5–14.5 dpc), infectious viral particles were not detected
595 in fetuses, and transcriptional activation was more restricted (139 upregulated, 1
596 downregulated), dominated by interferon-mediated pathways. This profile aligns with
597 increased placental maturity and antiviral competence, as reported for ZIKV-induced IFN
598 responses (40). The presence of infectious viruses in placenta and uterus, but not in fetal
599 tissues, suggests an effective placental barrier at this stage (39,41). The 50 shared
600 upregulated genes across gestational stages—mostly ISGs—reflect a conserved antiviral

601 signature, but timing-dependent transcriptional divergence underscores critical periods of
602 vulnerability, including disruption of angiogenic and developmental pathways (42) and
603 inflammatory responses characteristic of MAYV (23,35). Immunohistochemical analysis
604 provided complementary spatial evidence of MAYV localization in placental and fetal
605 tissues at mid gestation, supporting molecular and virological findings.

606 While direct extrapolation from murine models to humans is limited, these findings
607 provide a biologically plausible framework to explore potential maternal–fetal risks with
608 MAYV infection in human during pregnancy.

609 Limitations should be considered when interpreting these findings and their traslational
610 implications. Intraperitoneal inoculation does not fully recapitulate natural vector-borne
611 transmission and may influence early viral kinetics. Nevertheless, this route is widely
612 used in murine models of systemic arbovirus and alphavirus infection. Although
613 intraplantar models are well established for reproducing the articular and muscular
614 manifestations characteristic of Mayaro virus infection (23,24,35) intraperitoneal
615 administration was selected to minimize pain and distress in accordance with
616 internationally accepted animal welfare and refinement principles (43,44) while reducing
617 confounding effects related to local tissue injury and inflammation. This approach
618 facilitates a more controlled analysis of systemic viral kinetics and tissue tropism.

619 Although MAYV is primarily transmitted by mosquitoes (10), our results provide
620 preliminary evidence supporting the biological plausibility of a sexual transmission route,
621 which requires dedicated follow-up studies. Infectious particles were consistently
622 detected in testes and was found in sperm samples following cell culture-based
623 amplification, similar to long-term ZIKV RNA shedding in sperm (39). Two females
624 exposed to infected males became positive in reproductive tissues, though viral loads

625 were very low and RT-qPCR remained below detection limits. Males exposed to infected
626 females were mostly negative, except for one showing detectable viral titers in sperm.
627 These observations suggest that, if sexual transmission occurs, it may involve low-level
628 infections or limited replication in gonads, a known challenge in arbovirus detection (39).

629 *In vivo* imaging with MAYV-nLuc confirmed rapid dissemination at 24 hpi, with
630 persistent luminescence in limbs up to 10 dpi, supporting musculoskeletal tropism
631 (23,45). Infectious virus persisted in joints and muscle—sites associated with arthralgia
632 in humans (18,46) and luminescence without PFU detection in older animals suggests
633 persistence of viral RNA or subgenomic RNA after infectious virus is cleared. Younger
634 mice (4-week-old) showed persistent infectious particles in peripheral tissues, consistent
635 with increased susceptibility at early ages. This *in vivo* imaging experimental model can
636 be used effectively for a non-invasive longitudinal monitoring of viral replication over a
637 10-day period capturing both acute disease and early recovery phases reported (23,35).
638 In this context, the model represents a robust experimental platform for vaccine or
639 therapeutics challenges studies, allowing quantitative assessment of *in vivo* infection
640 kinetics and intervention efficacy under controlled conditions.

641

642 # Conclusion

643 This study establishes a robust murine model that reveals the systemic dissemination,
644 tissue tropism of MAYV, while supporting its potential for expanded transmission
645 pathways. Our findings demonstrate that gestational timing is a key determinant of
646 placental permissiveness and fetal exposure during acute infection, identifying early

647 pregnancy as a window of heightened vulnerability. The detection of infectious viral
648 particles in reproductive tissues and sperm further supports the biological plausibility of
649 non-vector transmission routes, although dedicated follow-up studies are required. By
650 integrating virological, hematological, transcriptomic, histological, and *in vivo* imaging
651 approaches, this work provides a comprehensive framework to advance the understanding
652 of MAYV pathogenesis and to perform future studies addressing maternal–fetal infection
653 and transmission dynamics.

654

655 # References

656 1. Organización Panamericana de la Salud / Organización Mundial de la Salud. Alerta
657 Epidemiológica: Fiebre de Mayaro. 1 de mayo de 2019, Washington, D.C.:
658 OPS/OMS;2019 [Internet]. Available from: www.paho.org

659 2. Blohm G, Elbadry MA, Mavian C, Stephenson C, Loeb J, White S, et al. Mayaro
660 as a Caribbean traveler: Evidence for multiple introductions and transmission of
661 the virus into Haiti. International Journal of Infectious Diseases. 2019 Oct
662 1;87:151–3.

663 3. Ganjian N, Riviere-Cinnamond A. Mayaro virus in Latin America and the
664 Caribbean. Revista Panamericana de Salud Publica/Pan American Journal of
665 Public Health. 2020;44.

666 4. Valencia-Marín BS, Gandica ID, Aguirre-Obando OA. The Mayaro virus and its
667 potential epidemiological consequences in Colombia: An exploratory
668 biomathematics analysis. Parasit Vectors. 2020 Oct 8;13(1).

669 5. Brustolin M, Bartholomeeusen K, Rezende T, Ariën KK, Müller R. Mayaro virus,
670 a potential threat for Europe: vector competence of autochthonous vector species.
671 Parasit Vectors. 2024 Dec 1;17(1).

672 6. Celone M, Beeman S, Han BA, Potter AM, Pecor DB, Okech B, et al.
673 Understanding transmission risk and predicting environmental suitability for
674 Mayaro Virus in Central and South America. PLoS Negl Trop Dis. 2024 Jan
675 1;18(1).

676 7. García-Romero C, Carrillo Bilbao GA, Navarro JC, Martin-Solano S, Saegerman
677 C. Arboviruses in Mammals in the Neotropics: A Systematic Review to Strengthen
678 Epidemiological Monitoring Strategies and Conservation Medicine. Vol. 15,
679 Viruses. MDPI; 2023.

680 8. Fundación iO. Aumento significativo de casos de fiebre Mayaro en Acre, Brasil
681 [Internet]. May 29, 2025 [cited 2025 Dec 14]. Available from:
682 https://fundacionio.com/aumento-significativo-de-casos-de-fiebre-mayaro-en-
683 acre-brasil/ [Internet]. [cited 2025 Oct 22]. Available from:
684 https://fundacionio.com/aumento-significativo-de-casos-de-fiebre-mayaro-en-
685 acre-brasil/

686 9. Andreolla AP, Borges AA, Bordignon J, Duarte dos Santos CN. Mayaro Virus:
687 The State-of-the-Art for Antiviral Drug Development. Vol. 14, Viruses. MDPI;
688 2022.

689 10. Diagne CT, Bengue M, Choumet V, Hamel R, Pompon J, Missé D. Mayaro virus
690 pathogenesis and transmission mechanisms. Vol. 9, Pathogens. MDPI AG; 2020.
691 p. 1–23.

692 11. Marinho M dos S, Ferreira GM, Grosche VR, Nicolau-Junior N, Campos T de L,
693 Santos IA, et al. Evolutionary Profile of Mayaro Virus in the Americas: An Update
694 into Genome Variability. Viruses. 2024 May 1;16(5).

695 12. Cereghino C, Roesch F, Carrau L, Hardy A, Ribeiro-Filho H V., Henrion-Lacritick
696 A, et al. The E2 glycoprotein holds key residues for Mayaro virus adaptation to the
697 urban Aedes aegypti mosquito. PLoS Pathog [Internet]. 2023 Apr 1 [cited 2025
698 Oct 22];19(4):e1010491. Available from:
699 https://pmc.ncbi.nlm.nih.gov/articles/PMC10109513/

700 13. Ribeiro-Filho H V., Coimbra LD, Cassago A, Rocha RPF, Guerra JV da S, de
701 Felicio R, et al. Cryo-EM structure of the mature and infective Mayaro virus at 4.4
702 Å resolution reveals features of arthritogenic alphaviruses. Nat Commun. 2021
703 Dec 1;12(1).

704 14. Mendonça DC, Reis EVS, Arias NEC, Valencia HJ, Bonjardim CA. A study of the
705 MAYV replication cycle: Correlation between the kinetics of viral multiplication
706 and viral morphogenesis. Virus Res [Internet]. 2022 Jan 2 [cited 2025 Oct
707 21];323:199002. Available from:
708 https://pmc.ncbi.nlm.nih.gov/articles/PMC10194297/

709 15. Krokovsky L, Lins CRB, Guedes DRD, Wallau G da L, Ayres CFJ, Paiva MHS.
710 Dynamic of Mayaro Virus Transmission in Aedes aegypti, Culex quinquefasciatus
711 Mosquitoes, and a Mice Model. Viruses. 2023 Mar 1;15(3).

712 16. Pereira TN, Virginio F, Souza JI, Moreira LA. Emergent Arboviruses: A Review
713 About Mayaro virus and Oropouche orthobunyavirus. Vol. 2, Frontiers in Tropical
714 Diseases. Frontiers Media SA; 2021.

715 17. De Thoisy B, Gardon J, Alba Salas R, Morvan J, Kazanji M. Mayaro virus in wild
716 mammals, French Guiana. Emerg Infect Dis. 2003 Oct 1;9(10):1326–9.

717 18. Silva-Ramos CR, Mejorano-Fonseca JA, Hidalgo M, Rodríguez-Morales AJ,
718 Faccini-Martínez ÁA. Clinical, Epidemiological, and Laboratory Features of
719 Mayaro Virus Infection: a Systematic Review. Vol. 10, Current Tropical Medicine
720 Reports. 2023. p. 309–19.

721 19. de Curcio JS, Salem-Izacc SM, Pereira Neto LM, Nunes EB, Anunciação CE,
722 Silveira-Lacerda E de P. Detection of Mayaro virus in Aedes aegypti mosquitoes
723 circulating in Goiânia-Goiás-Brazil. Microbes Infect. 2022 Jun 1;24(4).

724 20. Pancetti FGM, Honório NA, Urbinatti PR, Lima-Camara TN. Twenty-eight years
725 of Aedes albopictus in Brazil: A rationale to maintain active entomological and
726 epidemiological surveillance. Rev Soc Bras Med Trop. 2015;48(1):87–9.

727 21. Rosa RB, de Castro EF, de Oliveira Santos D, da Silva MV, Pena LJ. Mouse
728 Models of Mayaro Virus. Vol. 15, Viruses. Multidisciplinary Digital Publishing
729 Institute (MDPI); 2023.

730 22. da Silva Caetano CC, Camini FC, Almeida LT, Ferraz AC, da Silva TF, Lima RLS,
731 et al. Mayaro Virus Induction of Oxidative Stress is Associated With Liver
732 Pathology in a Non-Lethal Mouse Model. Sci Rep. 2019 Dec 1;9(1).

733 23. Mota MT de O, Costa VV, Sugimoto MA, Guimarães G de F, Queiroz-Junior CM,
734 Moreira TP, et al. In-depth characterization of a novel live-attenuated Mayaro virus
735 vaccine candidate using an immunocompetent mouse model of Mayaro disease.
736 Sci Rep. 2020 Dec 1;10(1).

737 24. de Carvalho AC, Dias CSB, Coimbra LD, Rocha RPF, Borin A, Fontoura MA, et
738 al. Characterization of Systemic Disease Development and Paw Inflammation in a
739 Susceptible Mouse Model of Mayaro Virus Infection and Validation Using X-ray
740 Synchrotron Microtomography. Int J Mol Sci. 2023 Mar 1;24(5).

741 25. Weger-Lucarelli J, Carrau L, Levi LI, Rezelj V, Vallet T, Blanc H, et al. Host
742 nutritional status affects alphavirus virulence, transmission, and evolution. PLoS
743 Pathog. 2019;15(11).

744 26. Powers AM, Aguilar P V, Chandler LJ, Brault AC, Meakins TA, Watts D, et al.
745 Genetic relationships among mayaro and Una viruses suggest distinct patterns of
746 transmission. 2006 Sep.

747 27. Chuong C, Bates TA, Weger-Lucarelli J. Infectious cDNA clones of two strains of
748 Mayaro virus for studies on viral pathogenesis and vaccine development. Virology
749 [Internet]. 2019 Sep 1 [cited 2025 Oct 27];535:227–31. Available from:
750 https://www.sciencedirect.com/science/article/pii/S0042682219301886?via%3Di
751 hub

752 28. Roszkowski M, Mansuy IM. High Efficiency RNA Extraction From Sperm Cells
753 Using Guanidinium Thiocyanate Supplemented With Tris(2-
754 Carboxyethyl)Phosphine. Front Cell Dev Biol [Internet]. 2021 Apr 21 [cited 2025
755 Oct 27];9:648274. Available from: www.frontiersin.org

756 29. Zhou Y, Zhou B, Pache L, Chang M, Khodabakhshi AH, Tanaseichuk O, et al.
757 Metascape provides a biologist-oriented resource for the analysis of systems-level
758 datasets. Nat Commun [Internet]. 2019 Dec 1 [cited 2025 Oct 27];10(1). Available
759 from: https://pubmed.ncbi.nlm.nih.gov/30944313/

30. Llamas-González YY, Campos D, Pascale JM, Arbiza J, González-Santamaría J. A Functional Ubiquitin-Proteasome System is Required for Efficient Replication of New World Mayaro and Una Alphaviruses. Viruses [Internet]. 2019 Apr 1 [cited 2025 Oct 27];11(4). Available from: https://pubmed.ncbi.nlm.nih.gov/31018496/

31. Valdés-Torres P, Campos D, Bhakta M, Galán-Jurado PE, Durant-Archibold AA, González-Santamaría J. Honokiol and Alpha-Mangostin Inhibit Mayaro Virus Replication through Different Mechanisms. Molecules. 2022 Nov 1;27(21).

32. Written WK. Modification of the oestrous cycle of the mouse by external stimuli associated with the male. 1956 Jul.

33. Figueiredo CM, Neris RL da S, Gavino-Leopoldino D, da Silva MOL, Almeida JS, dos-Santos JS, et al. Mayaro Virus Replication Restriction and Induction of Muscular Inflammation in Mice Are Dependent on Age, Type-I Interferon Response, and Adaptive Immunity. Front Microbiol. 2019 Oct 1;10.

34. Acosta-Ampudia Y, Monsalve DM, Rodríguez Y, Pacheco Y, Anaya JM, Ramírez-Santana C. Mayaro: an emerging viral threat? Vol. 7, Emerging Microbes and Infections. Nature Publishing Group; 2018.

35. Santos FM, Dias RS, de Oliveira MD, Costa ICTA, Fernandes L de S, Pessoa CR, et al. Animal model of arthritis and myositis induced by the mayaro virus. PLoS Negl Trop Dis. 2019 May 1;13(5).

36. Acosta-Ampudia Y, Monsalve DM, Rodríguez Y, Pacheco Y, Anaya JM, Ramírez-Santana C. Mayaro: an emerging viral threat? Vol. 7, Emerging Microbes and Infections. Nature Publishing Group; 2018.

782 37. Atkins GJ, Carter J, Sheahan3 BJ. Effect of Alphavirus Infection on Mouse
783 Embryos. Vol. 38, INFECTION AND IMMUNITY. 1982.

784 38. Taylor M, Rayner JO. Immune Response to Chikungunya Virus: Sex as a
785 Biological Variable and Implications for Natural Delivery via the Mosquito.
786 Viruses [Internet]. 2023 Sep 1 [cited 2025 Oct 27];15(9):1869. Available from:
787 https://pmc.ncbi.nlm.nih.gov/articles/PMC10538149/

788 39. Hcini N, Lambert V, Picone O, Carod JF, Carles G, Pomar L, et al. Arboviruses
789 and pregnancy: are the threats visible or hidden? Trop Dis Travel Med Vaccines.
790 2024 Dec 1;10(1).

791 40. Vermillion MS, Lei J, Shabi Y, Baxter VK, Crilly NP, McLane M, et al.
792 Intrauterine Zika virus infection of pregnant immunocompetent mice models
793 transplacental transmission and adverse perinatal outcomes. Nat Commun. 2017
794 Feb 21;8.

795 41. Megli CJ, Coyne CB. Infections at the maternal–fetal interface: an overview of
796 pathogenesis and defence. Vol. 20, Nature Reviews Microbiology. Nature
797 Research; 2022. p. 67–82.

798 42. Wu Y, Su K, Zhang Y, Liang L, Wang F, Chen S, et al. A spatiotemporal
799 transcriptomic atlas of mouse placentation. Cell Discov. 2024 Dec 1;10(1).

800 43. Directive - 2010/63 - EN - EUR-Lex [Internet]. [cited 2025 Dec 19]. Available
801 from: https://eur-lex.europa.eu/legal-content/EN/TXT/?uri=CELEX:32010L0063

802 44. Recognition and alleviation of pain in laboratory animals. National Academies
803 Press; 2009. 177 p.

45. Diagne CT, Bengue M, Choumet V, Hamel R, Pompon J, Missé D. Mayaro virus pathogenesis and transmission mechanisms. Vol. 9, Pathogens. MDPI AG; 2020. p. 1–23.

46. Santos FM, Dias RS, de Oliveira MD, Costa ICTA, Fernandes L de S, Pessoa CR, et al. Animal model of arthritis and myositis induced by the mayaro virus. PLoS Negl Trop Dis. 2019 May 1;13(5).

Acknowledgments

We thank José González Santamaría from the Department of Genomics and Proteomics Research, Gorgas Memorial Institute for Health Studies, Panama, for providing the primary antibody used in this study.

Author contributions

Conceptualization: APA, GM and MC. Methodology: APA, PP, JLP, MPG, BV, JMV, GM and MC. Investigation: APA, PP, JLP, MPG, GG, BV, JMV, GM and MC. Visualization: APA, PP, JLP, MPG, GG, BV, JMV, GM and MC. Statistical Analyses: APA. Supervision: GM and MC. Writing—original draft: APA, PP, JLP, GG, JH, AF, JMV, GM and MC. Writing—review & editing: APA, PP, JLP, MPG, GG, JH, AF, BV, JMV, GM and MC. Project administration: GM and MC. Funding acquisition: GM and MC. All authors agreed to submit the manuscript and have read and approved its final version. Authors take full responsibility for its content.

Funding

Institut Pasteur de Montevideo and FOCEM (COF 03/11), G4 program Institut Pasteur de Montevideo.

Competing interests

The authors declare no competing interests.